Mapping of the heavy ion outflows as seen by IMAGE and multifluid global modeling for the 17 April 2002 storm

R. M. Winglee

Department of Earth and Space Sciences, University of Washington, Seattle, Washington, USA

W. Lewis

Southwest Research Institute, San Antonio, Texas, USA

Gang Lu

High Altitude Observatory, National Center for Atmospheric Research, Boulder, Colorado, USA

[1]   Multifluid global modeling that includes both light and heavy ion dynamics is used to investigate changes in magnetospheric dynamics produced by enhanced ionospheric outflows for the 17 April 2002 storm. The predicted outflow rates and their effects on the magnetosphere are compared with AMIE and IMAGE/HENA data as a function of relative O^+ concentration in the ionosphere. It is shown that O^+ can be the dominant species on the dusk side in the inner magnetosphere during the periods of high activity even for ionospheric concentrations as low as 5% as a result of differential heavy ion convection patterns. However, for these low outflow conditions, the cross-polar cap potential is much larger than that calculated by AMIE. As the O^+ ionospheric concentration increases, the heavy outflow rate approaches canonical values, and the effective ionospheric resistivity falls in association with a decrease in cross-polar cap potential and an increase in the auroral field aligned currents. Within the magnetosphere, the region where the O^+ concentration exceeds 50% expands toward the duskside and down the tail. Pressures in excess of 1 nPa can be supported by the enhanced O^+ outflows. The presence of these enhanced outflows appears at about the same time and over a similar region to enhancements seen in the HENA 51–180 keV oxygen data. These results provide a direct tie between heavy ionospheric outflows and their energization in the tail and suggest that during this period the heavy ions provide a substantial amount of the plasma required to support the magnetotail current sheet. The model results also show that the enhanced O^+ outflow leads to the enhanced exclusion of light ions of both solar wind and ionospheric origin in the plasma sheet, albeit with the light ions experiencing enhanced heating in an O^+ dominated current sheet. These results indicate that observed heavy ionospheric outflows and their energetization in the tail have global consequences for the magnetosphere including supporting the dynamics of the tail current sheet during active times and in global circulation including the cross-polar cap potential and the region 1 and 2 currents.

Citation: Winglee, R. M., W. Lewis, and G. Lu (2005), Mapping of the heavy ion outflows as seen by IMAGE and multifluid global modeling for the 17 April 2002 storm, *J. Geophys. Res.*, *110*, A12S24, doi:10.1029/2004JA010909.

1.   Introduction

[2]   The issue of the relative importance of the solar wind and ionospheric plasma sources in the terrestrial magnetosphere has been debated for more than 2 decades. Initial observations of intense ionospheric flows were first reported by *Shelley et al.* [1972], who showed that during a magnetic storm the precipitating flux of keV O^+ ions could exceed that of H^+. Intense ionospheric outflows have been observed by a variety of spacecraft, including ISIS-1 and -2 [*Klumpar*, 1979], S3-3 [*Sharp et al.*, 1977; *Ghielmetti et al.*, 1978; *Gorney et al.*, 1981], DE-1 [*Waite et al.*, 1985; *Yau et al.*, 1985, 1988; *Moore et al.*, 1986; *Collin et al.*, 1987; *Roberts et al.*, 1987; *Pollock et al.*, 1990], and Akebono [*Yau et al.*, 1993] and Polar [*Peterson et al.*, 2001]. A compilation of these results was developed by *Yau and André* [1997], who showed ionospheric fluxes of between 10^{25} and 10^{26} H^+ ions/s and $5 \times 10^{24} - 5 \times 10^{26}$ O^+ ions/s as *Kp* increases from 1 to 6.

[3]   These ion outflow rates are sufficiently high that *Chappell et al.* [1987, 2000] proposed that ionospheric ions

could populate the plasma sheet. The adequacy of the ionospheric source can easily be demonstrated by calculating the rate at which the ionosphere can supply plasma and comparing that with an estimated rate at which plasma is injected from the solar wind. For a solar wind density of 6 cm^{-3} and a speed of 450 km/s there are about 7×10^{28} amu/s incident on the dayside magnetosphere. Depending on the efficiency of entry across the magnetopause, one might expect a few percent of the incident solar wind ions (i.e., of the order of 10^{27} amu/s) to cross into the magnetosphere. An O$^+$ outflow of 6×10^{25} ion/s for $Kp = 4$ would inject into the magnetosphere the same amu/s as the solar wind. In other words, heavy ionospheric outflows cannot be neglected. A question of equal importance to be addressed in this paper is access of these flows to critical regions of the magnetosphere where the strongest particle acceleration occurs.

[4] The importance of ionospheric outflow motivated *Moore* [1991] and *Moore and Delcourt* [1995] to propose the presence of a geopause, a boundary that demarcates the change in the sphere of influence from the ionospheric to solar wind. The geopause was envisaged to extend into at least the midtail region, as suggested by single particle tracking [*Delcourt et al.*, 1989, 1993]. The first three-dimensional (3-D) rendering of the geopause was made using the multifluid simulations [*Winglee*, 1998a, 1998b, 2000], which showed the boundary to be very dynamic. It is smallest for northward interplanetary magnetic field (IMF), when centrifugal acceleration [*Cladis*, 1986; *Horwitz*, 1987] of heavy ionospheric ions is inhibited by low convection speeds or, equivalently, by low cross-polar cap potential. Solar wind enters via high-latitude reconnection and is subsequently convected into the magnetosphere. For southward IMF, enhanced heavy ionospheric outflows can be driven by increases in the cross-polar cap potential, while entry of solar wind plasma is limited to the mantle, most of which does not have access to the inner plasma sheet.

[5] The presence of heavy ionospheric ions is important in the generation of energetic particle populations within the magnetosphere. For example, during storms, the oxygen concentration in the ring current can be comparable to, if not greater than that of H$^+$ [*Krimigis et al.*, 1985; *Hamilton et al.*, 1988; *Roeder et al.*, 1996]. More recently, Geotail observations have shown the presence of O$^+$ in both the midtail lobe/mantle [*Mukai et al.*, 1994] and in the distant tail [*Hirahara et al.*, 1996; *Seki et al.*, 1996]. A statistical study by *Seki et al.* [1998] showed that the lobe/mantle O$^+$ beams between 8 and 210 R_E have an average density during solar minimum of about 1×10^{-3} cm^{-3}, which corresponds to about 1.2% of the proton component. In addition, the oxygen ions appear to have been strongly energized, attaining energies up to about 3.5 keV. While 1.2% concentration may appear to be a small number, it should be noted that oxygen even at this level would provide nearly 20% of the mass to the tail and therefore cannot be considered negligible.

[6] However, there is equally compelling evidence that the solar wind also plays an important role in supplying plasma to the magnetosphere. *Lennartsson* [1987, 1992] has shown from ISEE 1 data that the plasma sheet always has a significant population of He^{2+} ions (indicating a nonnegligible contribution from the solar wind source). This popu-

lation was observed to be the largest during periods of extremely weak geomagnetic activity when the interplanetary magnetic field (IMF) was persistently northward. There are some data that suggest that the entry process may be mass dependent in that the He^{2+}/H$^+$ density ratio is observed to decrease by 40% from the magnetosheath to the low-latitude boundary layer [*Fuselier et al.*, 1997]. In addition, a substantial dawn/dusk asymmetry in the He^{2+}/H$^+$ density ratio [*Fuselier et al.*, 1997, 1999] adds further evidence for a mass-dependent entry process at the magnetopause. However, this mass-dependent entry has yet to be accounted for in any magnetospheric model. Transient increases in He^{2+}/H$^+$ density have been observed in association with storm activity [*Lui et al.*, 2000], indicating that He^{2+} is not necessarily impeded at the magnetopause.

[7] On the basis of their single particle tracking studies, *Ashour-Abdalla et al.* [1997, 1999], *Peroomian et al.* [2000], and *Peroomian* [2003] have argued for a significant solar wind source. On the other hand, single particle tracking by *Delcourt et al.* [1989, 1993, 1994] and *Chappell et al.* [2000] indicate a strong ionospheric source. *Winglee* [2003] have also used single particle tracking to assess the relative importance of solar wind and ionospheric sources. They demonstrated that while the magnetosphere is open to solar wind entry under storm conditions, the solar wind plasma has limited access to the midtail region where reconnection and strong particle acceleration is initiated. Light ions from the midnight auroral oval and heavy ions from the postmidnight sector can reach the tail current sheet, and under the resultant acceleration substantial dawn-dusk asymmetries in the energetic particle flows are produced. In addition, ion cyclotron effects were shown to have important consequences on the convection of different ion species within the magnetosphere and that even He^{++} and O^{6+} would undergo mass separation effects and not necessarily be a fully accurate tracer for solar wind entry into the magnetosphere.

[8] The reality is that there is strong mixing of both solar wind and ionospheric sources, and the relative amounts vary with solar wind conditions. In their study of the inner magnetosphere using CRRES, *Korth et al.* [2002] show that storm-time substorms can have O$^+$/H$^+$ ratios of several hundred percent while nonstorm-time substorms have O$^+$/H$^+$ ratios of 15–65%. Even for these values, O$^+$ is a significant factor in the total energy density. *Nosé et al.* [2000, 2001] have also noted an order of magnitude increase in the relative energy density of O$^+$ in the near-Earth region from quiet to storm times. Polar observations have demonstrated that O$^+$ outflow can have a prompt response to the arrival of a magnetic cloud event [*Moore et al.*, 1999, 2001]. *Peterson et al.* [2002] using Akebono, Polar, and FAST data showed that while the overall outflow rate as summarized by *Yau and André* [1997] were validated over an extended period, four orders of magnitude variation in the local outflow rates at all geomagnetic activity levels are typically observed. Examination of the ion composition of flux ropes showed the strong mixing of both solar wind (He^{2+}) and ionospheric ion components (O$^+$) with the relative amount of O$^+$ highly variable [*Lui et al.*, 1998].

[9] New global views of the transport of both light and heavy ions are becoming available through comparative studies using data from IMAGE spacecraft of auroral

emissions, which indicate precipitating particle populations, and neutral atom imaging, which is representative of trapped particle populations [Burch et al., 2001; Mitchell et al., 2001; Mende et al., 2002]. During a very well-observed substorm, Mende et al. [2002] showed that 20 min prior to onset, a decrease in auroral precipitation is observed, while the ENA intensity continues to increase. At onset the electron aurora can increase by an order of magnitude in intensity while the proton precipitation increases by only about 50%. These intensifications are short-lived (∼10 min), while the ENA enhancements can last for hours. Other ENA results show the rapid penetration of the solar wind electric field into the dayside magnetosphere within 10 min and reveal that the energy distribution of <27 keV particles is very different from >27 keV particles [Brandt et al., 2002a, 2002b]. Storm-time substorms show substantial enhancements in the production of energetic O^+ that are not seen in association with nonstorm substorms [Mitchell et al., 2003].

[10] This paper provides the first study in which the results of a multifluid model [Winglee, 2000, 2003, 2004] that explicitly incorporates H^+ and O^+ ionospheric outflow are compared with IMAGE/HENA observations [Mitchell et al., 2000], which reveal the spatial loading of energetic O^+ in the inner magnetosphere for the geomagnetic storm of 17 April 2002. Storms are examples of disturbed intervals with both large incident solar wind fluxes and strong ionospheric outflows, and as such provide key information on the ebb and flow of the different plasma sources within the magnetosphere. The April 2002 event was associated with substantial magnetospheric activity with a Kp of 7.

[11] The details of the model are described in section 2. Section 3 compares the model outflow rates with the outflow rates of Yau and André [1997]. This comparison demonstrates that the model outflow rates for the ionospheric plasma are of the correct order and that the outflows form hysteresis curves that yield a strong correlation of flux with auroral current, irrespective of whether the current is rising in association with increasing activity or falling as the IMF becomes more northerly. The presence of the O^+ outflows is shown to reduce the effective resistivity of the ionosphere.

[12] Section 4 shows that the buildup of hot O^+ in the magnetosphere in both spatial extent and timing occurs at approximately the same time and in about the same region as observed enhancements in HENA O 51−180 keV data. O^+ is found to be the dominant ion on the duskside in the inner magnetosphere during increasing activity even for the lowest outflow rates assumed here. For O^+ outflow rates near observed values, O^+ becomes the dominant component over much on the plasma sheet, leading to enhanced exclusion of the light ions from the plasma sheet. In this latter case, however, the energy of the light ions is enhanced compared with the case where the O^+ flux is relatively low. A summary of results is given in section 5.

2. Numerical Algorithm

[13] The multifluid treatment used here was initially developed to study magnetospheric/ionospheric coupling in the terrestrial magnetosphere [Winglee, 1998, 2002, 2003]. The work presented here uses the full form of the fluid equations, including ion cyclotron effects in the momentum equation [Winglee, 2004]. The inclusion of these effects is critical to capturing the dynamics of the reconnection region and the injection of the energetic plasma into the inner magnetosphere, which is being imaged by HENA. The details of the simulation model are as follows.

[14] The specific equations for mass, momentum and pressure for each component α are

$$\frac{\partial \rho_\alpha}{\partial t} + \nabla \cdot (\rho_\alpha \boldsymbol{V}_\alpha) = 0 \tag{1}$$

$$\rho_\alpha \frac{d\boldsymbol{V}_\alpha}{dt} = q_\alpha n_\alpha (\boldsymbol{E}_\alpha + \boldsymbol{V}_\alpha \times \boldsymbol{B}(r)) - \nabla P_\alpha - \left(\frac{GM_E}{R^2}\right)\rho_\alpha \vec{r} \tag{2}$$

$$\frac{\partial P_\alpha}{\partial t} = -\gamma \nabla \cdot (P_\alpha \boldsymbol{V}_\alpha) + (\gamma - 1)\boldsymbol{V}_\alpha \cdot \nabla P_\alpha \tag{3}$$

It is assumed that the electrons have sufficiently high mobility along the field lines that they are approximately in steady-state or drift motion (i.e., d/dt = 0) so that the momentum equation for the electrons reduces to

$$\boldsymbol{E} + \boldsymbol{V}_e \times \boldsymbol{B} + \frac{\nabla P_e}{en_e} = 0. \tag{4}$$

[15] Equation (4) is equivalent to the modified Ohm's law with Hall and grad P corrections included. Gravity is dropped in (4) since it has essentially no effect on the dynamics of the electrons. The rest of the electron dynamics are given by assuming quasi-neutrality, and applying the definitions for current, and electron pressure, i.e.,

$$n_e = \sum_i n_i, \quad \boldsymbol{V}_e = \sum_i \frac{n_i}{n_e}\boldsymbol{V}_i - \frac{\boldsymbol{J}}{en_e}, \quad \boldsymbol{J} = \frac{1}{\mu_0}\nabla \times \boldsymbol{B} \tag{5}$$

$$\frac{\partial P_e}{\partial t} = -\gamma \nabla \cdot (P_e \boldsymbol{V}_e) + (\gamma - 1)\boldsymbol{V}_e \cdot \nabla P_e, \tag{6}$$

and the evolution of the magnetic field by the induction equation

$$\frac{\partial \boldsymbol{B}}{\partial t} + \nabla \times \boldsymbol{E} = 0 \tag{7}$$

Substitution of (5) into (4) yields the modified Ohm's law of

$$\boldsymbol{E} = -\sum_I \frac{n_i}{n_e}\boldsymbol{V}_i \times \boldsymbol{B} + \frac{\boldsymbol{J} \times \boldsymbol{B}}{en_e} - \frac{1}{en_e}\nabla P_e + \eta(\boldsymbol{x})\boldsymbol{J} \tag{8}$$

[16] The first term in (8) is the ideal Ohm's law and the last term $\eta(\boldsymbol{x})\boldsymbol{J}$ is added to allow for finite conductivity in the ionosphere. Collisions beyond this region are assumed to be negligible. No anomalous resistivity is included in the code, as the nonideal terms included in (8) are sufficient to drive reconnection. Such corrections to the Ohm's law are known to be important in terrestrial reconnection studies

and can drive field-aligned currents into the auroral region [*Zhu and Winglee*, 1996, *Winglee et al.*, 1998; *Shay et al.*, 1998].

[17] The ion dynamics is determined by simultaneously time stepping all the individual ion species equations (i.e., (1)–(3)) using the electric field in (8). These equations are essentially the same as those used in hybrid codes except that the ions are treated in the fluid limit as opposed to particles in the hybrid code; both types of codes have fluid electrons. Thus hybrid codes have the advantage of full ion dynamics but a realistic 3-D hybrid model of the magnetosphere presently does not exist to the large computation resources needed to track a sufficiently large number of particles. The multifluid treatment can provide such a comprehensive treatment but does neglected to physics associated with the generation of high-energy tails in the ion distributions. The present modeling is enabled as a four-fluid system (one electron fluid, and solar wind H^+, ionospheric H^+, and ionospheric O^+ ion components).

[18] The equations are solved on a structured Cartesian grid using a two-step Lax-Wendroff differencing scheme [*Richtmyer and Morton*, 1967] with Lapidus smoothing on plasma properties only [*Sod*, 1978]. The latter is required to remove unphysical grid point oscillations across sharp discontinuities such as the bow shock. The grid spacing in the inner magnetosphere is 0.25 R_E and as such we are able to resolve heavy ion cyclotron dynamics in the magnetotail and magnetopause current sheets. In the midtail to distant tail, the grid spacing is increased steadily from 0.25 to about 3 R_E in the distant tail at x $\sim$ −200 R_E (GSM) and at the flanks at ±60 R_E. The solar wind boundary is at x = 35 R_E.

[19] The inner radius of the simulations is set to 2 R_E. The region within the inner boundary is given a finite resistance equivalent to a Reynolds number of 10. At the actual inner boundary (representing the ionosphere), the Reynolds number is increased to 20 and at one grid point above it is set at 40. At all other points the resistivity is zero. These values yield an overall height integrated resistance similar to that of the Earth's ionosphere. The parameter that shows the most sensitivity to controlling the ionospheric outflow rate is the assumed ionospheric density at the inner boundary. The density is assumed to consist of a fixed light ion density of 400 cm^{-3} at the inner boundary, with a temperature that varies from 20 eV at the equator to 0.1 eV at the poles. The high temperature at the equator represents the hotter plasma trapped on closed field lines versus the colder plasma that is present in the polar cap regions. Centrifugal acceleration leads to substantial energization (to several keV) beyond the imposed inner boundary temperatures. As such the results presented here are not sensitive to the assumed low boundary temperature conditions (assuming that the heating and acceleration of the ions is strongest in the tail as opposed to with the auroral regions alone). The results though are sensitive to the assumed relative density and as such processes at lower altitudes are crucial in increasing the scale height of O^+ up to radial distance where the global dynamics starts to control the ion energization. The model outflow rates are shown to be of order of the estimates of *Yau and André* [1997] so that the model does give plausible particle fluxes despite its relative simplicity.

[20] We perform simulations for three different relative concentrations of O^+: a 5% O^+, which is typical of quiet time conditions (case 1); 33% O^+ (case 2); and 66% O^+ (case 3). Cases 2 and 3 are consistent with storm time concentrations [cf. *Korth et al.*, 2002] with the changes in concentration initiated at 1330 UT after the passage of the shock and when the IMF turns strongly southward. For simplicity, the O^+ concentration is uniformly distributed around the inner radius. Test runs with variable O^+ concentration around the inner boundary do not show substantial differences. The main reason for this is that the model heavy ion outflow is dominated from the auroral and polar regions (as in the actual ionosphere). Thus the relative densities cited in the following are representative of high-latitude concentrations and not that over the equatorial regions, which typically remain low.

[21] We start each model run after the passage of the shock front of the magnetic cloud so that transient effects can be separated from longer-term storm conditions. It is shown that the heavy ion outflow for case 1 is significantly smaller than the outflow estimates given by *Yau and André* [1997]. The cross-polar cap potential for this case is also shown to be relatively high compared with the potential determined by assimilative mapping of ionospheric electrodynamics (AMIE) [e.g., *Lu et al.*, 2001]. As the O^+ relative density is increased, better agreement with *Yau and André* [1997] and AMIE is obtained, indicating the importance of including magnetospheric/ionospheric coupling in simulations of magnetospheric dynamics.

3. Solar Wind Conditions and the Global Magnetospheric Response

[22] Figure 1 shows the solar wind parameters as measured by the ACE spacecraft at L1. Prior to the arrival of the magnetic cloud, the solar wind conditions are typical of the slow solar wind with a density of about 8 cm^{-3} and a speed of about 350 km/s. With the arrival of the shock the solar wind density increases to about 60 cm^{-3} and a speed of about 500 km/s. After about 30 min from the arrival of the shock, the density declines to an almost constant value of about 25 cm^{-3} for several hours. Because of the extended elevated density, this storm represents an important test case for determining the relative importance of solar wind plasma since at these densities one would guess that the solar wind source should be the dominant source of plasma [*Borovsky et al.*, 1998].

[23] The corresponding evolution of the interplanetary magnetic field (IMF) is shown in Figure 2. The field associated with the magnetic cloud has a very strong dawn component of about 25 nT that lasts for about 4.5 hours after which it flips sign and becomes primarily duskward with an average magnitude of about 20 nT. The north/south component of the IMF is much more disturbed with periods of both strong northward and southward IMF up to about 1300 UT, after which it is primarily southward with a few short interval northward IMF periods every 30 to 40 min. The simulations presented in the following track the arrival of the cloud into the magnetosphere. Differences arising from changes in the ionospheric characteristics during the periods of extended southward IMF after 1330 UT are then studied in detail.

[24] The derived outflow rates are shown in Figure 3. The H^+ outflows of 10^{25} to 10^{26} ions/s are very similar in range
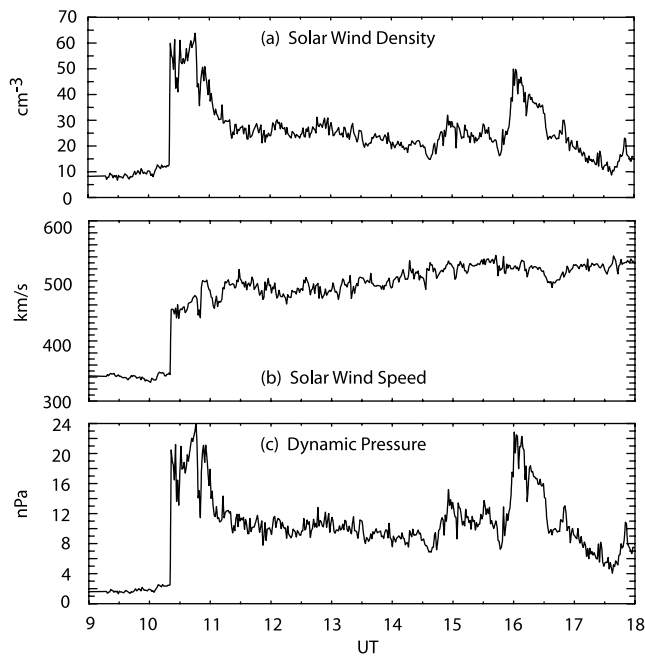
Figure 1. Evolution of the solar wind properties for the 17 April 2002 magnetic cloud event as measured by ACE at L1. The solar wind density is substantially elevated over nominal solar wind conditions after the magnetic cloud arrival.

to the statistical outflow rate of *Yau and André* [1997]. However, the O^+ outflow rate for case 1 (5% O^+ ionospheric relative density) remains at about 10^{25} ions/s, which is about an order of magnitude too small for the *Kp* 7 that occurred during the period. Cases 2 and 3 at relative densities of 33
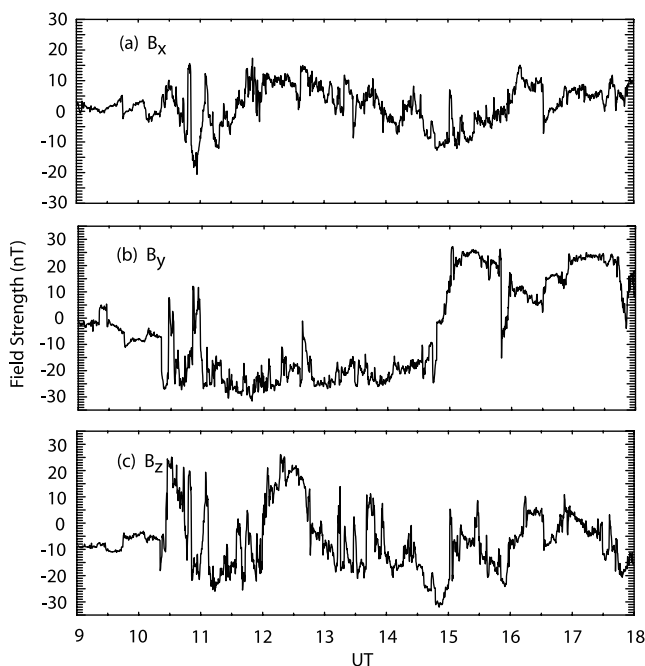
and 66% (initiated at 1330 UT) yield more realistic heavy ion outflow rates of about 10^{26} ions/s. Note that as the relative O^+ concentration is increased, the light ion outflow decreases even though the H^+ boundary conditions remain fixed. In other words, the heavy ion outflow at 10^{26} ions/s is sufficient to modify the overall dynamics of the magnetosphere [cf. *Winglee*, 2002].

[25] The presence of these large heavy ion outflows has important global effects on the magnetosphere. The global influence is illustrated in Figure 4a, which shows the evolution of the cross-polar cap potential for the event. Increasing the relative concentration of O^+ in the ionosphere can reduce the cross-polar cap potential by nearly 100 kV. This reduction in potential is easily understood since the solar wind only transfers a fixed amount of momentum to the magnetosphere. Because of the heavy ion outflows, more mass is added to the magnetosphere, and therefore the average velocity of the magnetospheric convection pattern decreases, which in turn causes the reduction in the cross-polar cap potential.

[26] For a reality check we have superposed AMIE results (dots) onto Figure 4a. Except for early times the potentials calculated by our simulations are about a factor of 2 higher than the AMIE results. For low O^+ concentrations our results are comparable to those from MHD simulations, which are typically a factor of 3 or higher than AMIE [*Fedder et al.*, 1998; *Raeder et al.*, 1998]. For higher O^+ concentrations, however, convergence between our results and the AMIE results is possible [cf. *Winglee*, 2004]. Note that the multifluid model tracks the AMIE results very closely in time. The main temporal
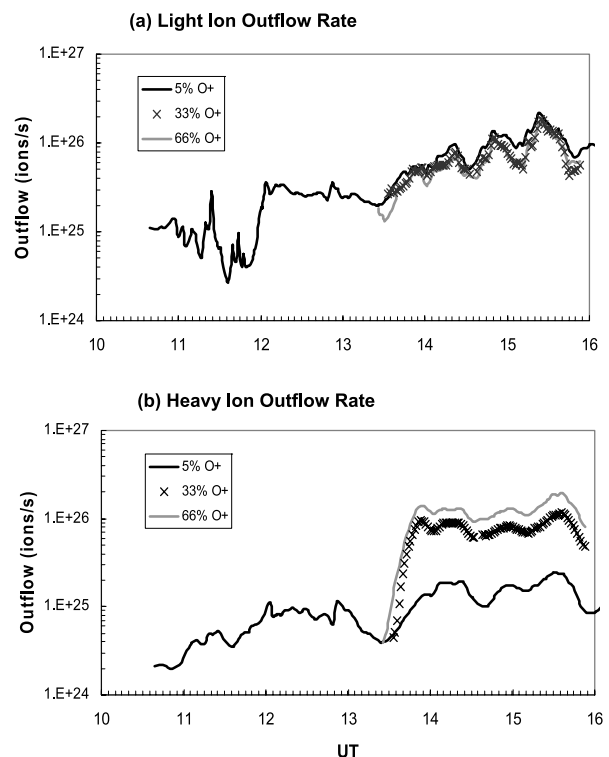

Figure 3. Variation of (a) light ion and (b) heavy ion outflow rates derived from the model as a function of time.

Figure 2. The evolution of the IMF. The period of interest is dominated by a strong dawnward IMF B_y, with IMF B_z.
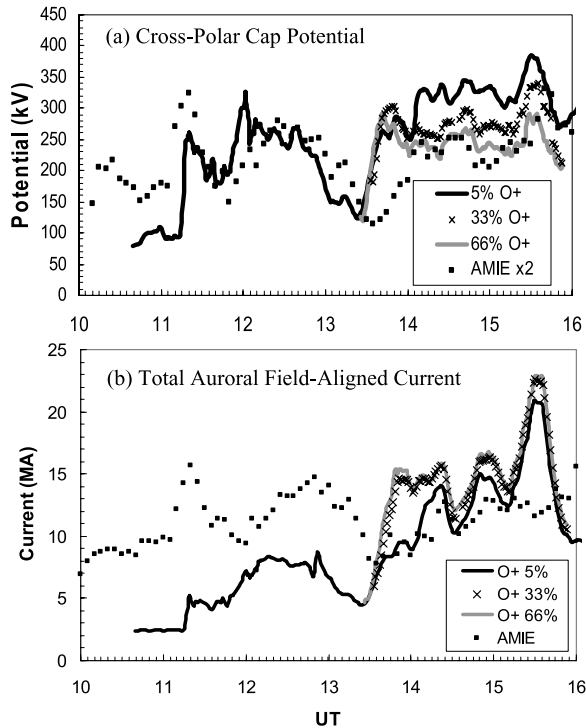
Figure 4. Variation of (a) the cross-polar cap potential and (b) the field-aligned aurora currents as a function of time.

difference is that the simulation responds too quickly to the southward IMF turning that produces the increase in potential at 1330 UT, which is indicative that we are underestimating the ionospheric outflow.

[27] The corresponding comparison of the total field-aligned currents into the auroral regions is shown in Figure 4b. The largest changes in the auroral currents appear at the arrival of the shock at the beginning of the event at 1120 UT. During the rest of the event the current inferred from AMIE is only about 50% more than the total of 8 MA for the prestorm conditions. This small change occurs in the presence of strongly (−15 nT) southward IMF and sustained solar wind densities of 20 cm^{-3} and solar wind speeds >500 km/s. On the other hand, the simulations clearly show a marked increase in the auroral currents in response to these changing solar wind conditions. The calculated current eventually increases toward the AMIE value during the period of extended southward IMF at times >1330 UT.

[28] Our simulations show that increasing the O$^+$ concentration enhances the field-aligned currents in the global model. This enhancement arises because increasing the O$^+$ density leads to mass loading of the field line at low altitudes, while during this initial loading phase the magnetospheric end of the field line has little heavy ion mass loading. As a result, the magnetospheric end of the field convects faster than the ionospheric end, which leads to enhanced twisting of the field line and hence larger field-aligned currents. A key result of this enhancement of the field-aligned current and the reduction of the cross-polar cap potential is that enhanced heavy ion outflows lead to a reduction in the effective resistance of the ionosphere. For this reason, heavy ionospheric

outflows cannot be neglected in the simulations studies of magnetosphere-ionosphere.

[29] In order to quantify the model outflows for comparison with those of *Yau and André* [1997], we replot the outflow rate as a function of integrated auroral current as a pseudo measure of auroral/magnetospheric activity. The comparison for the light ion outflows is shown in Figure 5. There are three key features to be seen from the figure. First, the current provides an excellent means of ordering the outflow data. Despite the variations in the IMF conditions that drive the auroral currents, the log of the light ion flux has an approximate linear dependence on the field-aligned current intensity similar to the linear dependence of the log of the *Yau and André* [1997] light ion flux on *Kp*. Second, the variation of the fluxes with IMF leads to hysteresis-like curves where the flux approximately recovers its value irrespective of whether the current is increasing with rising activity or with falling activity as the IMF becomes more northerly. The third feature is that the light ion flux decreases as the heavy ion concentration is increased. This decrease is associated with the reduction of the cross-polar cap and the overall convection speed within the magnetosphere.

[30] The corresponding outflow rates for the heavy ions are shown in Figure 6. The model results for the lowest concentration reaches a saturation value of ion outflow rate of 2×10^{25} ions/s for aurora currents greater than about 10 MA. This saturation value is very much smaller than the typical heavy ion outflow rates of *Yau and André* [1997]. As the O$^+$ concentration is increased, the outflow flux increases to values comparable to those reported by *Yau and André* [1997], and the saturation value increases to about $1-2 \times 10^{26}$ ions/s and occurs for auroral currents greater than about 15 MA. The net result is that the overall dependence of the heavy ion outflow rate on magnetospheric activity described by *Yau and André* [1997] can only be accounted for in the present model by allowing for a variable heavy ion concentration in the ionosphere that increases with magnetospheric/ionospheric activity.

4. Corresponding Magnetospheric Structures

[31] Of equal importance to characterizing the ion outflow rate as described in the previous section is question of the timing and position of the heavy ion outflows in the magnetosphere. In order to calibrate the model, the following shows a comparison of the model results with IMAGE/HENA 51−180 keV oxygen data. This comparison can be only considered qualitative since the model results primarily described the bulk characteristics of the O$^+$ at energies of only several keV while the HENA data is basically seen the high-energy tail of the O$^+$ ions generated by nonadiabatic processes. Despite the difference in energies, one expects an association between the two different data sets because the energetic O$^+$ ions must come from a seed population related to the bulk characteristics of the magnetospheric particle populations.

[32] For the comparison we an isosurface of the O$^+$ pressure at 1 nPa to provide a 3-D representation of hot O$^+$ in the magnetosphere. Pressure is chosen because it is a convolution of density and temperature and as such provides an approximate measure of O$^+$ flux. The value of
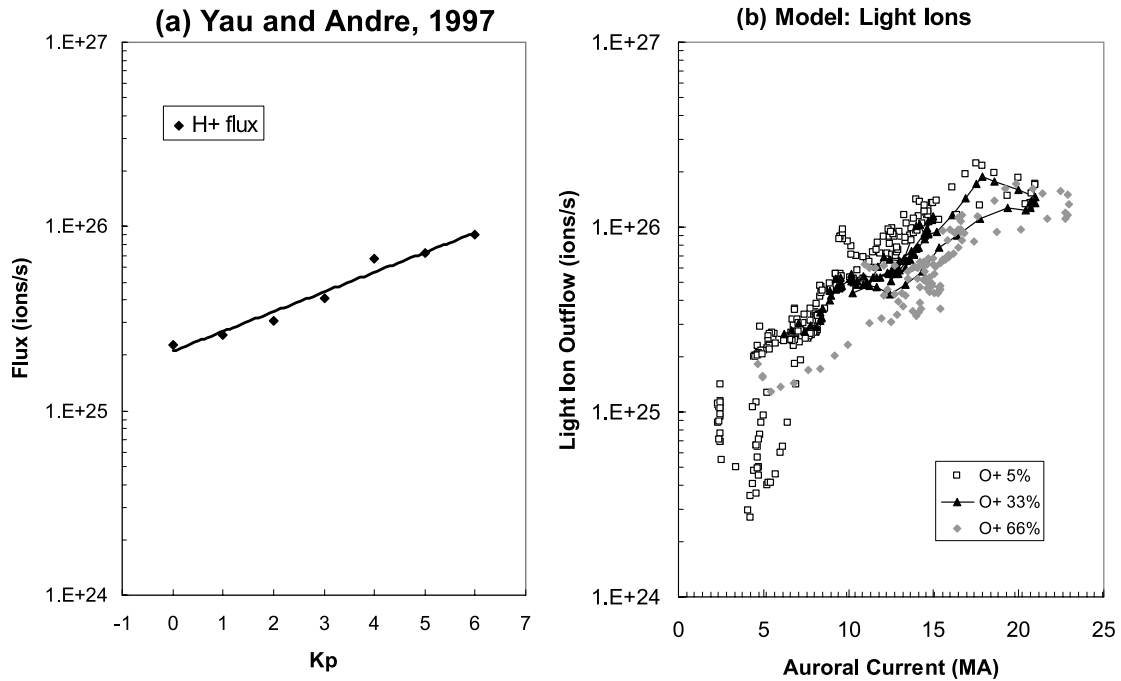
Figure 5. Correlation of the light ion outflows with respect to (a) *Kp* from *Yau and André* [1997] and (b) with the model field-aligned currents. The model outflows have a similar dependence with activity as seen in the results of *Yau and André* [1997] with increased heavy ionospheric densities reducing the overall light ion outflow rate.

1 nPa is chosen as it represents a value well above quiet time level, and for it to be obtained not only does the O^+ density have to be enhanced but the O^+ ions have also to be heated to several keV (the exact temperatures obtained are discussed at the end of the section). This data is compared with the HENA 51–180 keV O data [*Mitchell et al.*, 2000].

[33] Figure 7 shows the comparison case 3 (66% O^+ concentration). This case maximizes the O^+ influence on the
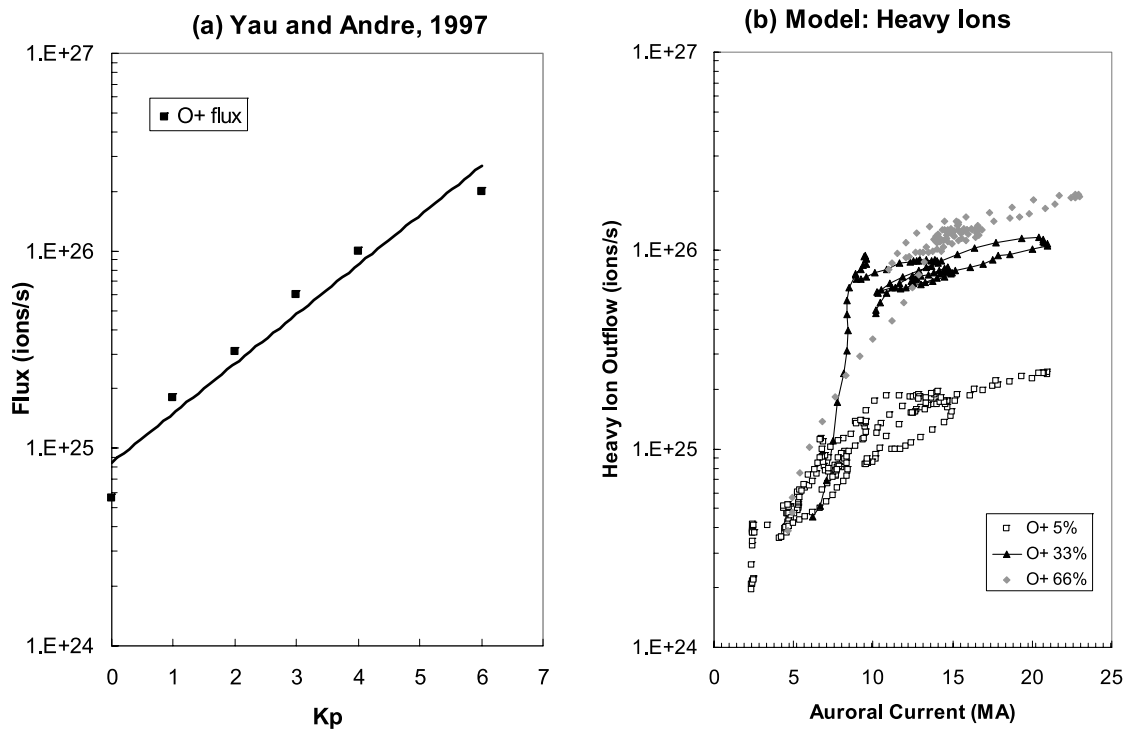

Figure 6. As in Figure 5 except for the heavy ions. An increase in the relative heavy ion concentration density at the inner boundary is required to produce an outflow rate that is comparable to that of *Yau and André* [1997].
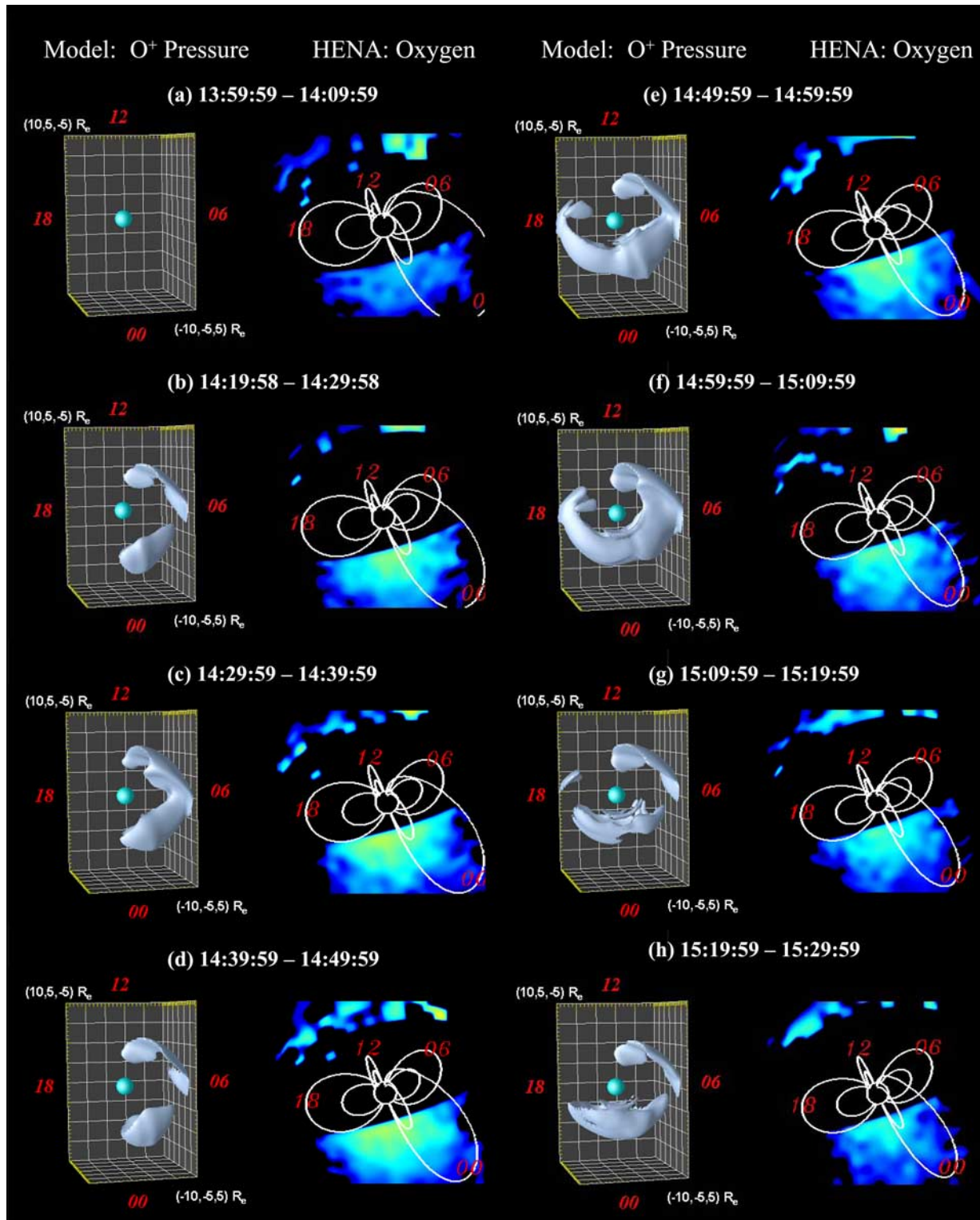
Figure 7. Comparison of the build up of O⁺ pressure around the Earth as derived from the modeling and as seen from IMAGE O⁺ HENA data over 1.5 hours for the 17 April 2002 storm event. The model is able to produce O⁺ features similar to those seen in the HENA images in both time and space.

magnetosphere, as already seen by the magnitude of the heavy ion outflows described in the previous section. It should be noted that the innermost region around the Earth is obscured by limitations of the model and the instrumentation, and therefore the interpretation is strictly limited only to the outer regions. For the model, as already noted the inner radius is 2 R_E, so views of energetic populations at near this inner boundary is unreliable. For HENA, the sharp end of the image near the Earth is produced by the Sun-shutter, which prevents the Sun from coming into the field of view but also prevents low-altitude emissions from being observed.

[34] Initially, the model O^+ pressure is insufficient to register, and the HENA data shows only weak emissions in the tail (Figure 7a). Starting at about 1420 UT and continuing to 1500 UT, there is a buildup of O^+ in the tail that is seen in both the model and HENA data (Figures 7b–7f). This energization is associated with an extended period of southward IMF. Following this period, there is a fading of O^+ in both model and HENA data associated with a more northerly IMF (Figures 7g and 7h). In other words, the model outflows are present at approximately the same time and over approximately the same region (at least outward from a few R_E) as the HENA data, indicating that the model results could potentially account for the seed population for the energetic O^+. This means that we now have the capacity to look at the effects of heavy ion outflows on the dynamics and structure of the magnetosphere.

[35] A crucial question is whether the solar wind or ionospheric plasma is controlling the plasma dynamics in the magnetosphere. As noted in the introduction, there is substantial uncertainty because of the conflicting data. Figure 8 shows the entry of the solar wind for the low O^+ ionospheric density case (case 1), which maximizes solar wind entry, as will be demonstrated below. The sequence shown in the figure starts about 10 min before the increase in HENA emissions to emphasize the dynamics of the solar wind plasma. Leading up to the HENA intensification, the solar wind density in the magnetosphere (Figures 8a and 8b) is decreasing. This decrease is associated with strong southward IMF. Coincident with the HENA intensification (Figure 8c), strong solar wind density entry from the dawn flanks is seen (associated with a more northerly IMF) while its density on the dusk flank continues to decrease on the dusk flanks. The HENA data indicate that the strongest O^+ emissions are on the duskside. The solar wind density in the tail continues to increase (Figure 8d) and the strongest HENA emissions move further toward dusk. In other words, while there is strong solar wind entry it is not in the same region where the strongest HENA emissions are observed.

[36] The issue of which plasma component is dominant is addressed in Figure 9, which shows the relative O^+ density corresponding to Figure 8. As the solar wind component decreases, there are local enhancements in the O^+ relative density that exceed 50% both in the inner magnetosphere on the dawnside and on the middle magnetosphere on the dusk flanks. These high concentrations are generated despite the fact that the O^+ density in the ionosphere is only 5%. As the solar wind enters from the dawnside, the regions of high relative O^+ concentration propagate across to the duskside. This is consistent with current sheet dawn-dusk acceleration. At the last time shown the pockets of high O^+

concentration in the middle magnetosphere have all but been overwhelmed, but the inner magnetosphere still has a region of O^+ plasma that moves around the duskside consistent with the HENA data. In other words, even for the low O^+ density case the bright regions of HENA emissions appear in the model as ones where the O^+ density is relatively high.

[37] The influence of O^+ density on the magnetosphere becomes increasingly important as the ionospheric O^+ density is increased, as illustrated in Figure 10. The left-hand panels show the O^+ density in absolute number density (top) and relative number density (bottom) for the low O^+ ionospheric case. The right-hand side shows same quantities for the high O^+ ionospheric density case. The higher density of O^+ at the inner boundary drives higher O^+ density through the magnetosphere, which is consistent with the higher heavy ion outflow rates described in section 3. The crucial points illustrated by this figure are that the O^+ relative density in the magnetosphere can exceed the ionospheric relative density and that the model suggests that the HENA emissions originate from these enhanced O^+ regions. This result is independent of the assumed ionospheric density compositions, and only the magnitude of the increase is dependent on the assumed ionospheric characteristics.

[38] The increase in the relative density of O^+ seen in Figure 10 is due not only to an increase in the O^+ density but also to a decrease in the H^+ density. The reduction of the ionospheric H^+ outflow has already been noted in section 3. The spatial distribution of these ions as well as that for the solar wind protons is shown in Figure 11. For the low ionospheric density case, the solar wind dominates the plasma sheet, particularly on the dawnside, and ionospheric H^+ dominates the lobes and makes comparable contributions to the duskside plasma sheet. For the high ionospheric O^+ density case (right-hand side), the contributions of these ions in terms of absolute density retreat to the dawnside. Thus the heavy ions modify the overall structure of the magnetosphere, including solar wind entry.

[39] While the access of light ions to the plasma sheet is reduced for high O^+ outflow rates, the temperature of the light ions that are able to reach the plasma sheet is substantially enhanced. This effect is shown in Figure 12, which compares light and heavy ion temperatures for the low and high O^+ outflow cases. For the low ionospheric density case, the hottest ions appear on the duskside, with the light ions having bulk temperatures of less than 1 keV. The temperatures of the light ions in the inner magnetosphere increase as the ions are convected into the dayside and into stronger magnetic field, reaching a peak temperature of about 2 keV. The heavy ions also have the highest temperatures on the duskside in the inner magnetosphere. In addition, a hot band of O^+ is seen stretching down the postmidnight sector of the plasma sheet.

[40] For the high O^+ ionospheric density case, an increase to a few keV is seen in the light ions, and the hot plasma regions extend farther down the tail and farther across into the dawn sector. This preferential heating of the light ions in the presence of relatively high heavy ion densities is also seen in auroral acceleration processes. The present simulations show that such processes are also relevant for the magnetotail. In latter case when the heavy ions become the
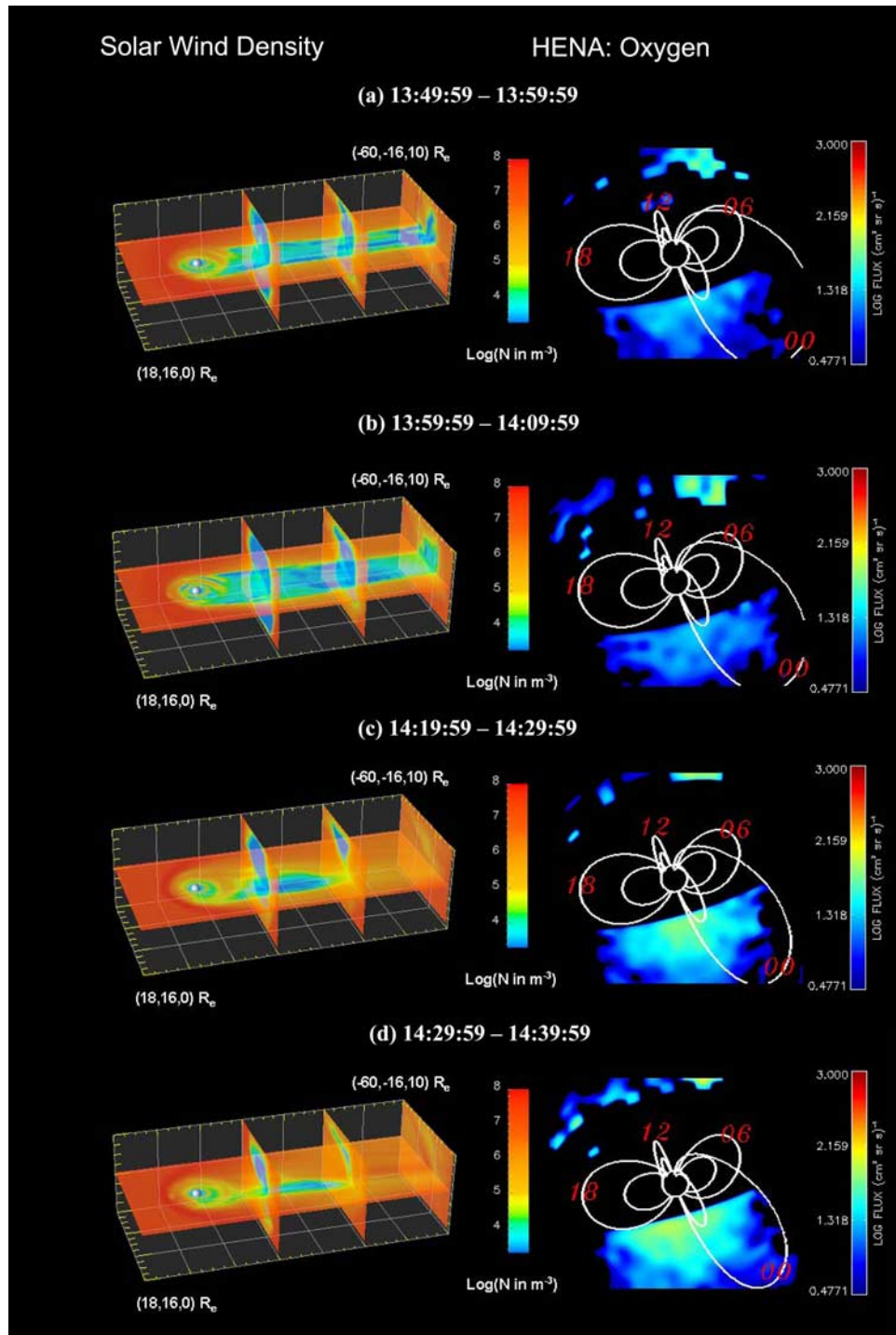
Figure 8. Evolution of the solar wind density out to the middle magnetosphere relative to the HENA data for the low O^+ ionospheric case. Prior to the HENA intensification, the density of solar wind plasma inside the magnetosphere declines. As the HENA emissions increase, there is enhanced solar wind entry on the dawnside, and this plasma entry remains dawnward of the HENA peak intensity.

dominant species in the tail, they can modify the overall structure of the current sheet. As demonstrated above, the heavy ions under the influence of current sheet acceleration produce stronger dawn-dusk asymmetries than would occur in a predominantly light ion current sheet. Light ions moving in this modified current clearly have different trajectories and attain different energies than are attained

in a predominantly light ion current sheet as seen in Figure 12.

5. Summary and Conclusions

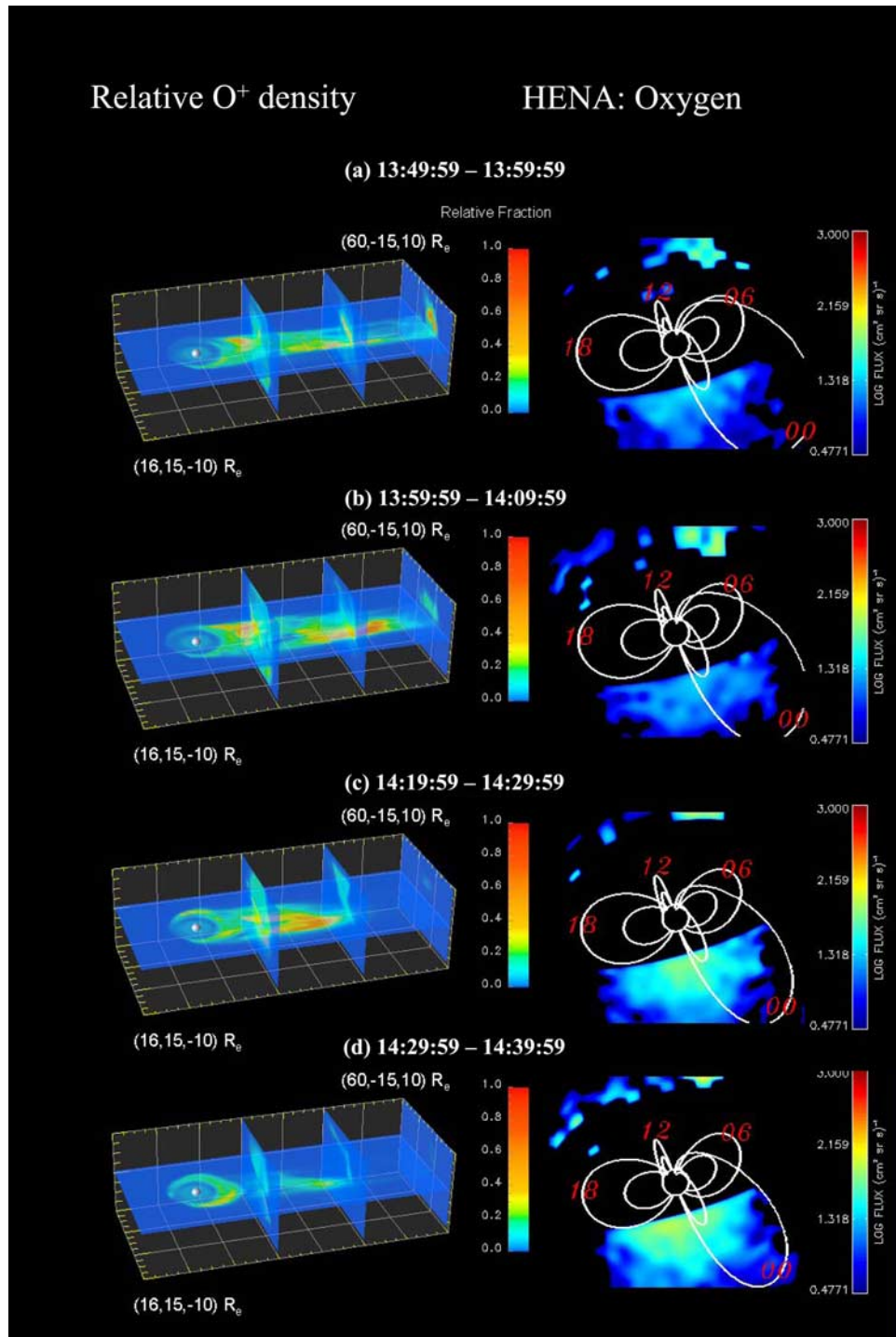[41] This paper provides the first comparison of HENA O^+ data with global multifluid modeling. Previous multi-

Figure 9. Same as in Figure 8, except the relative O^+ concentration is shown. Regions of enhanced O^+ density (Figures 8a and 8b) expand as the solar wind density in Figure 8 decline. The HENA intensification itself is correlated with a local region of enhanced O^+ concentration in the inner magnetosphere.

fluid modeling results have indicated that enhanced O^+ outflows can lead to the modification of the global dynamics of the magnetosphere, including the saturation of the cross-polar cap potential. Here the HENA data provides an important opportunity to test whether the global model is able to predict the spatial extent and timing of the heavy ionospheric outflows associated with storm activity. The comparison suggests that the heavy ion outflows from the model and their subsequent energization in the tail occur at about the correct time and position to be able to produce the seed population required to generate the HENA emissions. Such compar-
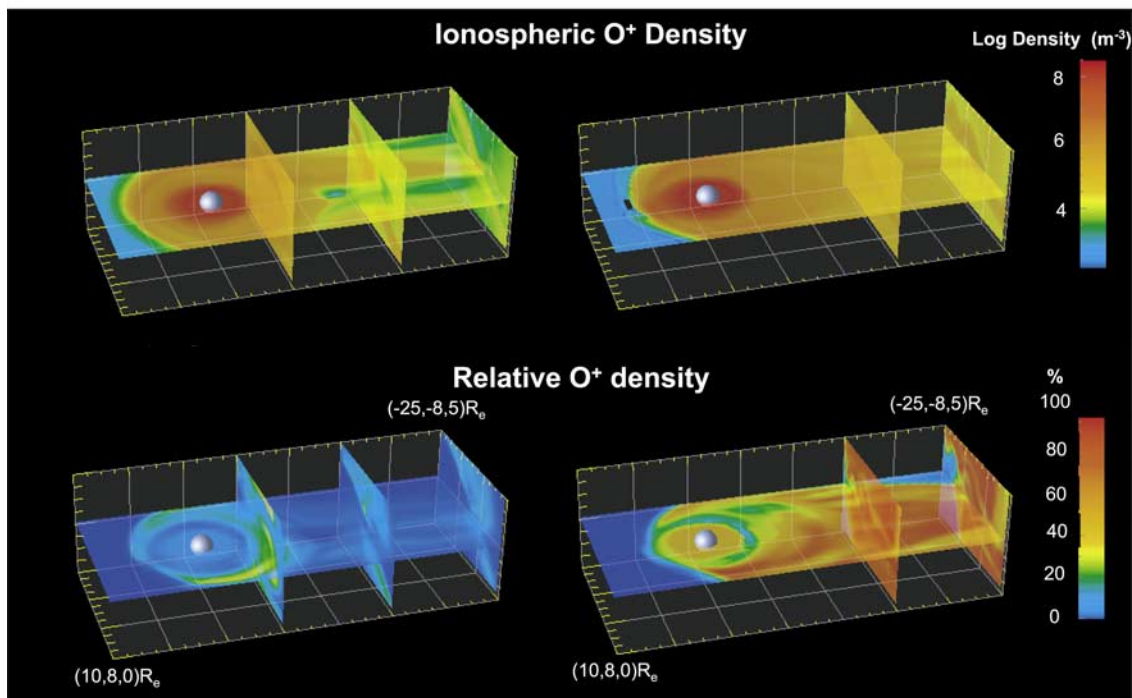
Figure 10. Absolute and relative density of the O^+ ions at 1450 UT. For the low relative concentration of 5% (left-hand side), magnetospheric processes lead to concentration of the O^+ density on the duskside that exceeds 30%. As the O^+ density in the ionosphere is increased, the dominance of O^+ increases across much of the plasma sheet and lobes.
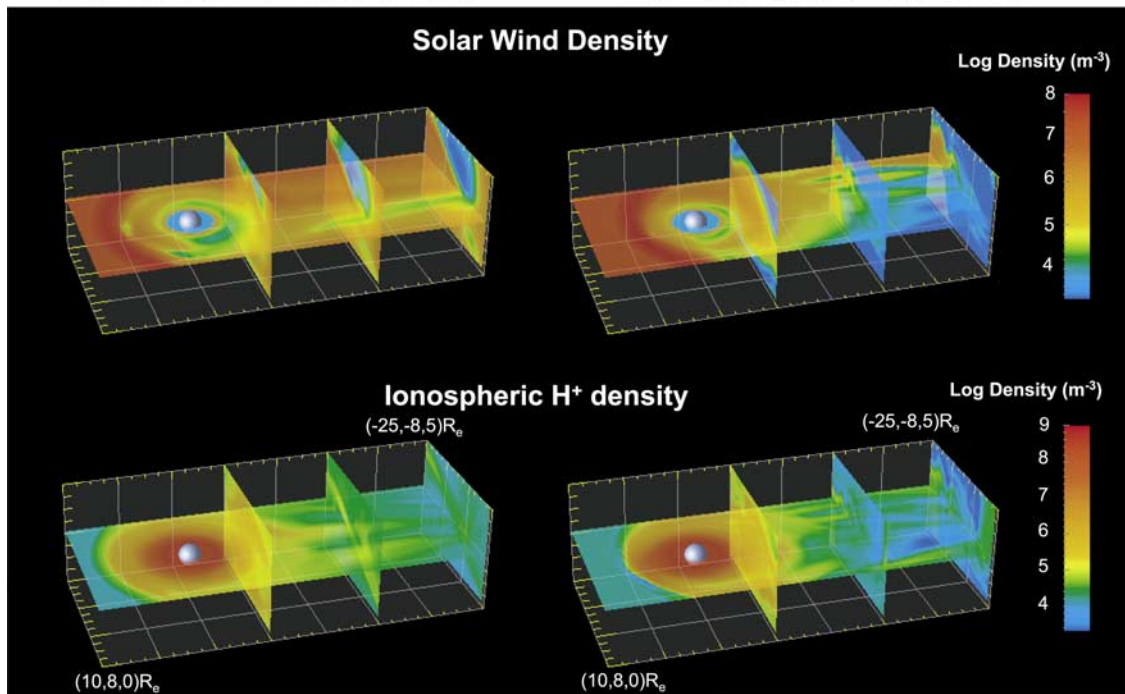

Figure 11. Changes in the solar wind and ionospheric H^+ density for the same time as in Figure 10 for the low (high) O^+ density concentration case on the left (right). Increasing the O^+ density produces reductions in the density of both sources of light ions in the bulk of the magnetosphere.
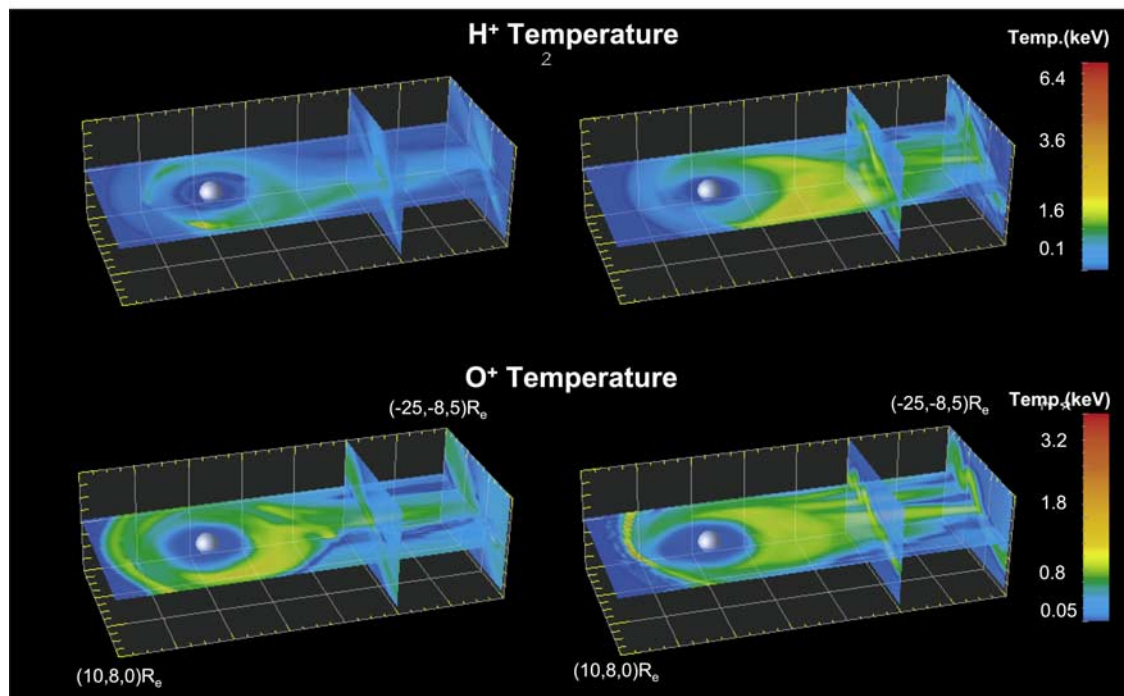
Low Ionospheric Outflow Case   **High Ionospheric Outflow Case**

Figure 12. Temperature of the light and heavy ions corresponding to Figures 10 and 11. While increased ionospheric outflow leads to reductions in the relative and absolute density of the light ions, the H+ ions that are present have an elevated temperature.

isons provide a useful tool for delving more fully into how heavy ionospheric outflow may be modifying the dynamics/structure of the magnetosphere.

[42] The case study presented here is for the storm of 17 April 2002, where substantial O^+ was observed in the HENA data. The simulations investigate the change in the properties of the ionospheric outflow and dynamics of the magnetosphere for three case of O^+ relative density in the ionosphere: (1) 5%, (2) 33%, and (3) 66 %. It is shown that the low ionospheric case yields heavy ionospheric outflow rates about an order of magnitude smaller than the statistical average outflow for the $Kp = 7$ that occurred during the event. The cross-polar cap for this case is about 3–4 times higher than that calculated by AMIE. The higher O^+ ionospheric concentrations bring the heavy ion outflow flux into agreement with the expected flux for the event, while dropping the cross-polar cap potential closer in line with AMIE and at the same time increasing the field-aligned currents.

[43] The key results from the study are the following:

[44] 1. The mass loading of the tail by heavy ionospheric outflows seen in the models occurs approximately at the same time and over approximately the same region as the development of energetic O as seen by HENA. This suggests that the model outflows are able to account for the seed population required to account for the HENA data.

[45] 2. The energetization of the model heavy ionospheric outflow in the tail can lead to pressures in excess of 1 nPa in the magnetosphere. This means that during disturbed times the O^+ ions are an important influence in supporting the tail current sheet.

[46] 3. The hot O^+ ions preferentially load the duskside of the magnetosphere, under the influence of current sheet acceleration. This preferential flow can lead to increases in the O^+ relative density several times greater than the ionospheric concentration. The region of dominant O^+ influence increases both down the tail and toward the dawn sector as the ionospheric outflow increases.

[47] 4. The regions of highest HENA emissions occur not only in regions of enhanced O^+ density but also in regions that are depleted of solar wind plasma. Southward IMF aids in limiting access of the solar wind plasma to the plasma sheet, and during such times ionospheric outflow is critical to maintaining the plasma required to support the current sheet.

[48] 5. The presence of high ionospheric outflow aids in the exclusion of the light ions of both solar wind and ionospheric origin to the plasma sheet. This is a new result and shows the importance of trying to separate out the relative importance of ionospheric and solar wind plasmas, i.e., in trying to isolate the geopause.

[49] 6. The exclusion of light ions from the plasma sheet leads to higher temperatures of the light ions that are able to reach the plasma sheet under these conditions. This preferential heating arises because when the heavy ions are the dominant component of the plasma, they control the bulk flow rate and the light ions experience stronger scattering under these slow flow but thin current sheet conditions.

[50] 7. The log of the outflow rate is linearly dependent on the auroral field-aligned current. This dependence occurs irrespective of whether the current is rising with increased activity or falling as the IMF becomes more northerly so

that the outflow rate essentially tracks a hysteresis-like curve when plotted against auroral activity.

[51] In summary, this paper continues the investigation of heavy ion interactions in the magnetosphere. The HENA data show the timing and spatial extent of hot heavy ion populations. The global multifluid modeling accounts for the presence of these hot populations in terms of enhanced heavy ion ionospheric outflows. The evidence presented here demonstrates that heavy ions can significantly control the dynamics/structure of the magnetosphere, contributing to the exclusion of solar wind plasma to the magnetosphere, modifying the convection rate, and altering the composition of energetic particle populations.

References

Ashour-Abdalla, M., et al. (1997), Ion sources and acceleration mechanisms inferred from local distribution functions, *Geophys. Res. Lett.*, *24*, 955.

Ashour-Abdalla, M., M. El-Alaoui, V. Peroomian, R. J. Walker, J. Raeder, L. A. Frank, and W. R. Paterson (1999), Source distributions of substorm ions observed in the near-Earth magnetotail, *Geophys. Res. Lett.*, *26*, 955.

Borovsky, J. E. (1998), The driving of the plasma sheet by the solar wind, *J. Geophys. Res.*, *103*, 17,617.

Brandt, P. C., S. Ohtani, D. G. Mitchell, R. Demajistre, and E. C. Roelof (2002a), ENA observations of a global substorm growth-phase dropout in the nightside magnetosphere, *Geophys. Res. Lett.*, *29*(20), 1962, doi:10.1029/2002GL015057.

Brandt, P. C., D. G. Mitchell, Y. Ebinhara, B. R. Sandel, E. C. Roelof, J. L. Burch, and R. Demajistre (2002b), Global IMAGE/HENA observations of the ring current: Examples of rapid response to IMF and ring current-plasmasphere interaction, *J. Geophys. Res.*, *107*(A11), 1359, doi:10.1029/2001JA000084.

Burch, J. L., D. G. Mitchell, B. R. Sandel, P. C. Brandt, and M. Wuest (2001), Global dynamics of the plasmasphere and ring current during magnetic storms, *Geophys. Res. Lett.*, *28*, 1159.

Chappell, C. R., T. E. Moore, and J. H. Waite Jr. (1987), The ionosphere as a fully adequate source of plasma for the earth's magnetosphere, *J. Geophys. Res.*, *92*, 5896.

Chappell, C. R., B. L. Giles, T. E. Moore, D. C. Delcourt, P. D. Craven, and M. O. Chandler (2000), The adequacy of the ionospheric source in supplying magnetospheric plasma, *J. Atmos. Sol. Terr. Phys.*, *62*, 421.

Cladis, J. B. (1986), Parallel acceleration and transport of ions from polar ionosphere to plasma sheet, *Geophys. Res. Lett.*, *13*, 893.

Collin, H. K., W. K. Peterson, and E. G. Shelley (1987), Solar cycle variation of some mass dependent characteristics of upflowing beams of terrestrial ions, *J. Geophys. Res.*, *92*, 4757.

Delcourt, D. C., C. R. Chappell, T. E. Moore, and J. H. Waite Jr. (1989), A three-dimensional numerical model of ionospheric plasma in the magnetosphere, *J. Geophys. Res.*, *94*, 11,893.

Delcourt, D. C., J. A. Sauvaud, and T. E. Moore (1993), Polar wind ion dynamics in the magnetotail, *J. Geophys. Res.*, *98*, 9155.

Delcourt, D. C., T. E. Moore, and C. R. Chappell (1994), Contribution of low energy ionospheric protons to the plasma sheet, *J. Geophys. Res.*, *99*, 5681.

Fedder, J. A., S. P. Linker, and J. G. Lyon (1998), A comparison of global numerical simulation results to data for the January 27–28, 1992, geospace environment challenge event, *J. Geophys. Res.*, *103*, 14,799.

Fuselier, S. A., E. G. Shelley, and O. W. Lennartsson (1997), Solar wind composition charges across the Earth's magnetopause, *J. Geophys. Res.*, *102*, 275.

Fuselier, S. A., R. C. Elphic, and J. T. Gosling (1999), Composition measurements in the dusk flank magnetosphere, *J. Geophys. Res.*, *104*, 4515.

Ghielmetti, A. G., R. G. Johnson, R. D. Sharp, and E. G. Shelley (1978), The latitudinal, diurnal, and altitudinal distributions of upflowing energetic ions of ionospheric origin, *Geophys. Res. Lett.*, *5*, 59.

Gorney, D. J., A. Clarke, D. Croley, J. F. Fennell, J. Luhmann, and P. Mizera (1981), The distribution of ion beams and conics below 8000 km, *J. Geophys. Res.*, *86*, 83.

Hamilton, D. C., G. Gloeckler, F. M. Ipovitch, W. Studenmann, B. Wilken, and G. Kremser (1988), Ring current development during the great geomagnetic storm of February 1986, *J. Geophys. Res.*, *93*, 14,343.

Hirahara, M., T. Mukai, T. Terasawa, S. Machida, Y. Saito, T. Yamamoto, and S. Kokubun (1996), Cold dense ion flows with multiple components observed in the distant tail lobe by Geotail, *J. Geophys. Res.*, *101*, 7769.

Horwitz, J. L. (1987), Core plasma in the magnetosphere, *Rev. Geophys.*, *25*, 579.

Klumpar, D. M. (1979), Transversely accelerated ions: An ionospheric source of hot magnetospheric ions, *J. Geophys. Res.*, *84*, 4229.

Korth, A., R. H. W. Friedel, F. Frutos-Alfaro, C. G. Moukis, and Q. Zong (2002), Ion composition of substorms during storm-time and non-storm-time periods, *J. Atmos. Sol. Terr. Phys.*, *64*, 561.

Krimigis, S. M., G. Gloeckler, R. W. McEntire, T. A. Potemra, F. L. Scarf, and E. G. Shelley (1985), Magnetic storm of September 4, 1984: A synthesis of ring current spectra and energy densities measured with AMPTE/CCE, *Geophys. Res. Lett.*, *12*, 329.

Lennartsson, W. (1987), Plasma sheet ion composition at various levels of geomagnetic and solar activity, *Phys. Scr.*, *36*, 367.

Lennartsson, W. (1992), A scenario for solar wind penetration of Earth's magnetic tail based on ion composition data from the ISEE 1 spacecraft, *J. Geophys. Res.*, *97*, 19,221.

Lu, G., A. D. Richmond, J. M. Ruohoniemi, R. A. Greenwald, M. Hairston, F. J. Rich, and D. S. Evans (2001), An investigation of the influence of data and model inputs on assimilative mapping of ionospheric electrodynamics, *J. Geophys. Res.*, *106*, 417.

Lui, A. T. Y., D. J. Williams, R. W. McEntire, S. P. Christon, T. E. Eastman, T. Yamamoto, and S. Kokubun (1998), Ion composition and charge state of energetic particles in flux ropes/plasmoids, *J. Geophys. Res.*, *103*, 4467.

Lui, A. T. Y., D. J. Williams, R. W. McEntire, S. P. Christon, A. B. Galvin, and D. J. Knipp (2000), Possible storm-intensity enhancing factor for the November 3, 1993 magnetic storm, *Adv. Space Res.*, *25*, 1639.

Mende, S. B., H. U. Frey, T. J. Immel, D. G. Mitchell, P. C:son Brandt, and J. C. Gerard (2002), Global comparison of magnetospheric ion fluxes and auroral precipitation during a substorm, *Geophys. Res. Lett.*, *29*(12), 1609, doi:10.1029/2001GL014143.

Mitchell, D. G., et al. (2000), High energy neutral atom (HENA) imager for IMAGE, *Space Sci. Rev.*, *91*, 67.

Mitchell, D. G., K. C. Hsieh, C. C. Curtis, D. C. Hamilton, H. D. Voss, E. C. Roelof, and P. C. Brandt (2001), Imaging two geomagnetic storms in neutral atoms, *Geophys. Res. Lett.*, *28*, 1151.

Mitchell, D. G., P. C. son Brandt, E. C. Roelof, D. C. Hamilton, K. C. Retterer, and S. Mende (2003), Global imaging of O^+ from IMAGE/HENA, *Space Sci Rev.*, *109*, 63.

Moore, T. E. (1991), Origins of magnetospheric plasma, *Rev. Geophys.*, *29*, 1039.

Moore, T. E., and D. C. Delcourt (1995), The geopause, *Rev. Geophys.*, *33*, 175.

Moore, T. E., M. Lockwood, J. H. Waite Jr., M. O. Chandler, W. K. Peterson, D. Wiemer, and M. Sugiura (1986), Upwelling O^+ source characteristics, *J. Geophys. Res.*, *91*, 7019.

Moore, T. E., W. K. Peterson, C. T. Russell, M. O. Chandler, M. R. Collier, H. L. Collin, P. D. Craven, R. Fitzenreiter, B. L. Giles, and C. J. Pollock (1999), Ionospheric mass ejection in response to a CME, *Geophys. Res. Lett.*, *26*, 2339.

Moore, T. E., M. O. Chandler, M. C. Fok, B. L. Giles, D. C. Delcourt, J. L. Horwitz, and C. J. Pollock (2001), Ring currents and internal plasmas, *Space Sci. Rev.*, *95*, 555.

Mukai, T., M. Hirahara, S. Machida, Y. Saito, T. Terasawa, and A. Nishida (1994), Geotail observation of cold ion streams in the medium distance magnetotail lobe in the course of a substorm, *Geophys. Res. Lett.*, *21*, 1023–1026.

Nosé, M., A. T. Y. Lui, S. Ohtani, B. H. Mauk, R. W. McEntire, D. J. Williams, T. Mukai, and K. Yumoto (2000), Acceleration of oxygen ions of ionospheric origin in the near-Earth magnetotail during substorms, *J. Geophys. Res.*, *106*, 7669.

Nosé, M., S. Ohtani, K. Takahashi, A. T. Y. Lui, R. W. McEntire, D. J. Williams, S. P. Christon, and K. Yumoto (2001), Ion composition of the near-Earth plasma sheet in storm and quiet intervals: Geotail/EPIC measurements, *J. Geophys. Res.*, *106*, 8391.

Peroomian, V. (2003), The influence of the interplanetary magnetic field on the entry of solar wind ions into the magnetosphere, *Geophys. Res. Lett.*, *30*(7), 1407, doi:10.1029/2002GL016627.

Peroomian, V., M. Ashour-Abdalla, and L. M. Zelenyi (2000), Dynamical properties of self-consistent magnetotail configurations, *J. Geophys. Res.*, *105*, 18,807.

Peterson, W. K., H. L. Collin, A. W. Yau, and O. W. Lennartsson (2001), POLAR/TIMAS observations of suprathermal ion outflow during solar minimum conditions, *J. Geophys. Res.*, *106*, 6059.

Peterson, W. K., H. L. Collin, M. Boehm, A. W. Yau, C. Cully, and G. Lu (2002), Investigation into the spatial and temporal coherence of ionospheric outflow of January 9–12, 1997, *J. Atmos. Sol. Terr. Phys.*, *64*, 1659.

Pollock, C. J., et al. (1990), A survey of upwelling ion event characteristics, *J. Geophys. Res.*, *95*, 18,969.

Raeder, J., J. Berchem, and M. Ashour-Abdalla (1998), The Geospace Environment Modeling grand challenge: Results from a global geospace circulation model, *J. Geophys. Res.*, *103*, 14,787.

Richtmyer, R. D., and K. W. Morton (1967), *Difference Methods for Initial Value Problems*, p. 300, Interscience, New York.

Roberts, W. T., et al. (1987), Heavy ion density enhancements in the outer plasmasphere, *J. Geophys. Res.*, *92*, 13,499.

Roeder, J. L., J. F. Fennell, M. W. Chen, M. Schulz, M. Grande, and S. Livi (1996), CRRES observations of the composition of the ring-current ion populations, *Adv. Space Res.*, *17*, 17.

Seki, K., M. Hirahara, T. Terasawa, I. Shinohara, T. Mukai, Y. Saito, S. Machida, T. Yamamoto, and S. Kokubun (1996), Coexistence of Earth-origin O^+ and solar wind-origin H^+/He^{++} in the distant magnetotail, *Geophys. Res. Lett.*, *23*, 985.

Seki, K., M. Hirahara, T. Terasawa, T. Mukai, Y. Saito, S. Machida, T. Yamamoto, and S. Kokubun (1998), Statistical properties and possible supply mechanisms of tailward cold O^+ beams in the lobe/mantle regions, *J. Geophys. Res.*, *103*, 4477.

Sharp, R. D., R. G. Johnson, and E. G. Shelley (1977), Observations of an ionospheric acceleration mechanism producing energetic (keV) ions normal to the geomagnetic field direction, *J. Geophys. Res.*, *82*, 3324.

Shelley, E. G., R. G. Johnson, and R. D. Sharp (1972), Satellite observations of an ionospheric acceleration mechanism, *J. Geophys. Res.*, *77*, 6104.

Shay, M. A., J. F. Drake, R. E. Denton, and D. Biskamp (1998), Structure of the dissipation region during collisionless magnetic reconnection, *J. Geophys. Res.*, *103*, 9165.

Sod, G. A. (1978), A survey of several finite difference methods for systems of nonlinear hyperbolic conservation laws, *J. Comput. Phys.*, *27*, 1.

Speiser, T. W. (1965), Particle trajectories in model current sheets: 1. Analytical solutions, *J. Geophys. Res.*, *70*, 4219.

Waite, J. H., Jr., et al. (1985), Escape of suprathermal O^+ ions in the polar cap, *J. Geophys. Res.*, *90*, 1619.

Winglee, R. M. (1998a), Multi-fluid simulations of the magnetosphere: The identification of the geopause and its variation with IMF, *Geophys. Res. Lett.*, *25*, 4441.

Winglee, R. M. (1998b), Imaging the ionospheric and solar wind sources in the magnetosphere through multi-fluid global simulations, *Phys. Space Plasmas*, *15*, 345.

Winglee, R. M. (2000), Mapping of ionospheric outflows into the magnetosphere for varying IMF conditions, *J. Atmos. Sol. Terr. Phys.*, *62*, 527.

Winglee, R. M. (2003), Circulation of ionospheric and solar wind particle populations during extended southward IMF, *J. Geophys. Res.*, *108*(A10), 1385, doi:10.1029/2002JA009819.

Winglee, R. M. (2004), Ion cyclotron and heavy ion effects on reconnection in a global magnetosphere, *J. Geophys. Res.*, *109*, A09206, doi:10.1029/2004JA010385.

Winglee, R. M., S. Kokubun, R. P. Lin, and R. P. Lepping (1998), Flux rope structures in the magnetotail: Comparison between Wind/Geotail observations and global simulations, *J. Geophys. Res.*, *103*, 135.

Yau, A. W., and M. André (1997), Source of ion outflow in the high latitude ionosphere, *Space Sci. Rev.*, *80*, 1.

Yau, A. W., P. H. Beckwith, W. K. Peterson, and E. G. Shelley (1985), Long-term (solar cycle) and seasonal variations of upflowing ionospheric ion events at DE 1 altitudes, *J. Geophys. Res.*, *90*, 6395.

Yau, A. W., W. K. Peterson, and E. G. Shelley (1988), Quantitative parameterization of energetic ionospheric outflow, in *Modeling Magnetospheric Plasma*, *Geophys. Monogr. Ser.*, vol. 44, edited by?, p. 211, AGU, Washington, D.C.

Yau, A. W., B. A. Whalen, C. Goodenough, E. Sagawa, and T. Mukai (1993), EXOSD (Akebono) observations of molecular NO^+ and N_2^+ upflowing ions In the high latitude auroral ionosphere, *Geophys. Res. Lett.*, *18*, 345.

Zhu, Z., and R. M. Winglee (1996), Tearing instability, flux ropes, and the kinetic current sheet kink instability in the Earth's magnetotail: A three-dimensional perspective from particle simulations, *J. Geophys. Res.*, *101*, 4885.

_____

W. Lewis, Southwest Research Institute, Division 15, San Antonio, TX 78228, USA. (wlewis@swri.edu)

G. Lu, High Altitude Observatory, National Center for Atmospheric Research, Boulder, CO 80307-3000, USA. (ganglu@ucar.edu)

R. M. Winglee, Department of Earth and Space Sciences, University of Washington, Seattle, WA 98195-1310, USA. (winglee@ess.washington.edu)